**Oktay Adıyaman**
Batman University, oktay.adiyaman@batman.edu.tr, Batman-Türkiye
**Musa Kılıç**
Batman University, musa.kilic@batman.edu.tr, Batman-Türkiye

| DOI | http://dx.doi.org/10.12739/NWSA.2023.18.4.2A0194 | |
|---|---|---|
| ORCID ID | 0000-0002-2674-3836 | 0000-0001-5808-6917 |
| Corresponding Author | Oktay Adıyaman | |

# AN ANALYTICAL RESEARCH OF CHIP COMPRESSION FACTOR IN ORTHOGONAL TURNING MECHANISM OF AISI 1050 STEEL

**ABSTRACT**

Numerous parameters are influential on-chip compression factor, surface roughness, and chip morphology. This experimental study investigated the effect of the chip compression factor on machinability. In this context, the influences of feed rate, cutting depth, rake angle, and chip slenderness ratio on-chip compression factor and surface roughness were investigated. Additionally, the orthogonal shear mechanism and shear strain were analyzed according to D'Alembert's principles of motion. The effect of parameters on the chip compression factor was analyzed with the help of the Matlab program according to the orthogonal cutting mechanism, shear strain, and D'Alembert's motion principles. It was observed that surface roughness increased steadily with increasing cutting depth and feed, but decreased linearly with rake angle and chip slenderness ratio values. According to the machinability criterion, the most appropriate chip slenderness ratio value was 15, but the chip compression factor value was between 1.7 and 2.3, which aligns with the literature results. Furthermore, concerning experimental and analytical values of both chip compression factor and shear strains, it was determined that the shearing process came true at a 35O shear angle in turning of AISI 1050 steel.

**Keywords:** Chip Compression Factor, Chip Slenderness Ratio, Vibration, Shear Angle, Chip Morphology

## 1. INTRODUCTION

In metal machining processes, as soon as the cutting edge contacts the workpiece, small fragments, named chips, start to be removed from the sample due to the plastic deformation effect. After the chips leave the machined sample, they pass on the rake face and then move away from the shear zone. This process is defined as chip formation. Generally, in metal-cutting processes, plastic deformation takes place within the shear plane. The severity level of the plastic deformation depends on the mechanical properties of the workpiece and the selected conditions. Chip Compression Factor (CCF), which is describable depending on the chip thickness or the chip length (with a broken cut), is a significant specifier for the plastic deformation level [1 and 2]. In machining operations, CCF can be evaluated as a machinability criterion, which also shows the severity level of plastic deformation [3]. Less plastic deformation shows better machinability and also the final shear strain identifies the severity of plastic deformation. Therefore, CCF indicates the real plastic deformation, which helps to reveal the consumed quantity of the energy in the shear zone, depending on the level of the shear strain [4]. At the beginning of the metal cutting process, chips are removed from the workpiece with higher shear angles due to the

temperature, taking place on the rake face. The source of this temperature is the friction between the cut chip and the rake face.

Additionally, this friction indicates the severity of the deformation of the removed chips [5]. As CCF increases, the shear angle decreases, and chip deformation severity elevates linearly. Undersized shear angles indicate a great amount of stress and a higher chip compression factor in the shear zone [6]. Moreover, CCF is a vital marker for chip morphology. However, when chip removal takes place in vibrating conditions, chip morphology cannot be evaluated, depending on CCF [7].

While carrying out machining operations, saw-toothed fragmented chip morphology is a hard problem to solve [8 and 9]. The chip in serration formation, especially the size of the pitch of the serration or saw-tooth, indicates the severity level of the stresses [10]. Furthermore, the quality of the machined surface and tool wear is influenced by the mechanism of the chip morphology [11]. The removed chips in serration formation can be ascribed to reiterated catastrophic shear instability due to the thermo-plasticity effect. This instability in the shear zone demonstrates the vibration level of the process [12]. Chips are removed from the workpiece in continuous shape at small feed rates and great rake angles, while they are fragmented form at high selected feed rates and small rake angles. Therefore, chip morphology is the chief identifier for the plastic strains, taking place in the shear zone during the machining operations [13]. The geometry of the cutting tool, especially the rake angle, has a direct effect on the strain levels in machining [10]. Rake angle leads to a reduction in the cutting forces and it affects the chip morphology. In other words, while the rake angle changes from negative values to positive, the chips are removed from the machined workpiece in serration formation [14]. Positive rake angles compensate for minor tensile strain, while negative rake angles lead to compressive strain during the machining. Moreover, negative rake angles trigger plastic deformation, resulting in poor surface quality and hard tool wear. Put differently, at higher selected rake angles, the intensity of the plastic deformation is diminished [11]. Rake angle is the most influential parameter on the remainder and compressive strains [15]. Therefore, when the rake angle of the tool rises, the chip size fragmentation density of the size of the chip serration decreases [7].    One of the second influential parameters on the chip morphology is the feed rate [16]. The feed rate and rake angle affect the compressive and remainder strains, linearly, but cutting depth does not have a significant impact [15]. However, the alteration temperature of the process and saw-tooth chip formation reduce with increasing the cutting depth and feed rate [10]. The periodical remainder strains determine the vibration frequency of the tool. Moreover, the topographic image of the machined surface can be associated with the frequency of the cutting tool vibration [17]. Furthermore, the chip removal rate depends on the feed rate, depth of cutting, and cutting speed; particularly, the thickness of the removed chip changes according to the severity of the vibration, in the direction of cutting depth [18]. Therefore, the generated fluctuations trigger the dynamic instability of the cutting tool [13]. At higher feed rates, both the length and shear angle of the removed chips decrease, and chips are removed from the machined sample in serration formation, with cracks and deformation marks, indicating the remainder strains. Accordingly, the feed rate is an influential parameter on plastic deformation, as well as on the shear strain [16]. The optimum ratio of cutting depth (the uncut chip width) to the feed rate should be selected to prevent the severity level of the deformation in the direction perpendicular to the cutting. For this purpose, cutting depth must be chosen higher than the feed rate, at a specific ratio. The severity of plastic deformation

decreases in the cutting-edge direction at a higher ratio of the cutting depth to the feed rate [19]. Numerous parameters influence the machinability. However, the ratio of the cutting depth to the feed rate, which is denominated as the CSR and the cutting edge approach angle has been studied so little that it is scarcely difficult to find any. The experimental results were evaluated according to conclusions like vibration, chip morphology, and surface roughness. Moreover, unlike the literature in this experimental study, the influence of CCF on machinability was investigated.

## 2. RESEARCH SIGNIFICANCE

Numerous parameters influence the machinability. However, the ratio of the cutting depth to the feed rate, which is denominated as the chip slenderness ratio (CSR) and the cutting edge approach angle has been studied [1 and 20]. These studies are so few that it is difficult to find any. Therefore, the chief objective of this paper is to investigate the influence of these vital parameters on the machining of AISI 1050 steel. The experimental results were evaluated according to parameters like vibration, chip morphology, and surface roughness. Moreover, unlike the literature, the influence of CCF on machinability was investigated in this experimental study. Moreover, the effect of parameters on CCF was analyzed with the help of the Matlab program according to the orthogonal cutting mechanism, shear strain, and D'Alembert's motion principles.

**Highlights:**
- There are few studies on the ratio of cutting depth to feed rate, called Chip Slenderness Ratio, and the cutting-edge approach angle.
- In this experimental study, unlike the literature, the effect of CCF on machinability was investigated.
- The influence of machining parameters on CCF was analyzed based on the orthogonal cutting mechanism, shear strain, and D'Alembert's principles of motion.

## 3. MATERIAL AND METHOD
### 3.1. CCF in Orthogonal Cutting Mechanism

In the orthogonal cutting mechanism, the cutting edge of the tool is perpendicular to the direction of the cutting tool proceeding. CCF can be evaluated depending on the geometrical relation between the uncut (t1) and the removed (tc) chips in the orthogonal cutting mechanism. Additionally, CCF can be analyzed geometrically depending on the shear angle (φ) and rake angle (α). As the cut chip is left from the machined workpiece, its geometrical dimensions change due to the shearing deformation, being the uncut chip exposed, during the machining process (Figure 1). CCF is derivable mathematically depending on shear (φ) and rake (α) angles, according to geometrical dimension as demonstrated in Figure 1.
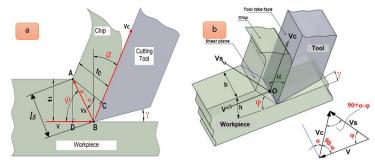


Figure 1. Chip formation in the orthogonal cutting mechanism a)2D b)3D

Uncut and removed chip thicknesses (t1) and (tc) derivable from the geometry in Figure 1 as seen in Equation 1.

$$t_1 = l_s * sin\varphi \quad \text{and} \quad t_c = l_s\cos(\varphi - \alpha) \tag{1}$$

CCF (λ) is achievable as the ratio of removed chip thickness (tc) to (t1) as seen in Equation 2 [21 and 22].

$$\frac{t_c}{t_1} = \lambda = \cos(\varphi - \alpha)/\sin\varphi \tag{2}$$

If Equation 2 is arranged trigonometrically, the shear angle can be formulated as in Equation 3, depending on the rake angle and CCF.

$$tan\varphi = \frac{cos\alpha}{\lambda - sin\varphi} \tag{3}$$

Furthermore, if Equation 3 is arranged depending on the shear and chip angles, CCF will be derivable as demonstrated, in Equation 4.

$$\lambda = \frac{cos\alpha}{tan\varphi} + sin\varphi \tag{4}$$

The relationship between cutting, chip and shear velocities associated with shear and chip angles is shown in Equation 5 according to the geometric shape of Figure 1 [23].

$$\frac{Vs}{V} = \frac{Cos(\alpha)}{Cos(\varphi - \alpha)} \qquad \frac{Vc}{V} = \frac{Sin(\varphi)}{\cos(\varphi - \alpha)} \qquad Vc = \frac{V}{\lambda} \tag{5}$$

The conversion of CCF concerning shear and chip angles is displayed in Figure 1. Figure 1 shows the effect of the shear angle and the chip angle on the CCF. According to Equation 4, the effects of shear and chip angles on CCF were analyzed with the help of the Matlab program. In the analysis, the shear angle (φ) was chosen between 15°-45° degrees, and the chip angle (α) was 0°-20°. As can be seen in the graphs of Figure 1, the CCF regularly decreases with increasing shear angle, while the CCF increases with increasing chip angle. However, the effect of chip angle on CCF is less than that of shear angl

### 3.2. CCF and Shear Strain in Orthogonal Cutting Mechanism

In machining operations, shear strain is a crucial specifier for the severity of the shear deformation. Figure 2 shows that the chips, which are removed from the workpiece by the cutting tool, are formed in the form of flowing plates over the rake face of the cutting tool. In Figure 2, the flow of removed chips is demonstrated on the rake face. The geometry of shear strain, depending on shear and rake angles, is also displayed in Figure 2.
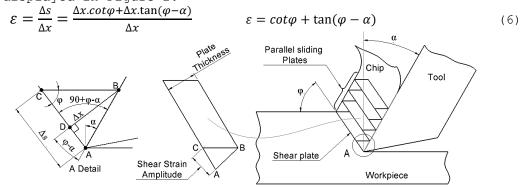
$$\varepsilon = \frac{\Delta s}{\Delta x} = \frac{\Delta x.cot\varphi + \Delta x.tan(\varphi - \alpha)}{\Delta x} \qquad \varepsilon = cot\varphi + tan(\varphi - \alpha) \tag{6}$$



Figure 2. Shear strain mechanism in orthogonal cutting (parallel sliding chip plates and geometry of shear strain)

According to the shear (φ) and rake (α) angles, the shear strain (ε) can be written the as ratio of (s) to (x) as seen in Equation 6. Depending on CCF and rake angle, the Merchant's shear strain can be calculated as in Equation 7 by substituting Equation 3 into Equation 5.

$$\varepsilon = \frac{1 - 2\lambda\sin(\alpha) + \lambda^2}{\lambda\cos(\alpha)} = \frac{\cos(\alpha)}{\cos(\varphi - \alpha)\sin(\varphi)} \tag{7}$$

### 3.3. D'Alembert's Principle of Chip Motion on the Rake Face

As soon as the chips break in the shear zone, they flow over the rake face of the tool and then they move away from the environment as seen in Figure 3.
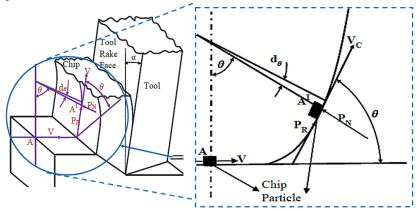


Figure 3. Geometry of D'Alembert's principle of chip motion on the rake face

The flow motion of the chip was examined geometrically according to D'Alembert's motion principle. Since the friction between the chip and the tool is active on the rake face of the cutting tool, according to the principle of D'Alembert, CCF was investigated depending on the friction coefficient and rake angle. Depending on uncut and removed chip thicknesses, CCF can be specified as seen in Equation 8.

$$\lambda = \frac{t_c}{t_1} = \frac{V_c}{V} \tag{8}$$

The volume of the uncut and removed chips per minute is equal to each other (Equation) 9.

$$V.t_1.b = V_c.t_c.b \tag{9}$$

The removed chips acted over the rake face of the cutting tool according to conventional static forces, which are specifiable with PR and PN as friction and normal forces, respectively. According to D'Alembert's principle, friction and normal forces can be classified depending on the chip mass, friction coefficient, and cutting speed, as seen in Equation 10.

$$m.\frac{dv}{dt} = -P_R = -\mu.P_N \tag{10}$$

With the first derivative of the linear velocity concerning time (dv/dt) the declaration equation is derived. Furthermore, the centrifugal force can be pointed out mathematically as seen in Equation 11.

$$m.\frac{v^2}{r} = P_N = m.v.\frac{d\theta}{dt} \tag{11}$$

Equation 12 can be derived from the correlation solution of (10) and Equation 11.

$$\frac{dv}{dt} = -\mu.v.\frac{d\theta}{dt} \tag{12}$$

By integrating Equation 12, the ratio of chip velocity to shear rate is achieved as shown in Equation 13 depending on the friction coefficient.

$$\frac{V_c}{V} = e^{-\mu\theta} \tag{13}$$

The geometry of D'Alembert motion principle is shown in Figure 3, where the chip is the angle ($\theta$) equal to ($\pi/2-\alpha$) that is drawn from the workpiece in the shear zone until it leaves the environment by flowing over the cutting tool rake face. Namely, angle ($\theta$) results in while the removed chip moves from point A to $A^I$ as demonstrated in Figure 3. Therefore, Equation 13 can be regulated as in Equation 14.

$$\frac{V_c}{V} = e^{(-\mu(\frac{\pi}{2}-\alpha))} \tag{14}$$

By correlation solving Equation 8 and Equation 14, the value of CCF is written as demonstrated in Equation 15 depending on the coefficient of friction according to D'Alembert principle.

$$\lambda = e^{(-\mu(\frac{\pi}{2}-\alpha))} \tag{15}$$

### 3.4. Experimental Setup in Turning Operations

A CNC turning machine was employed for the experiments. During the machining operations, the removed chips were gathered with the help of a metallic box, and fastened upon the body of the CNC machine as shown in Figure 4.
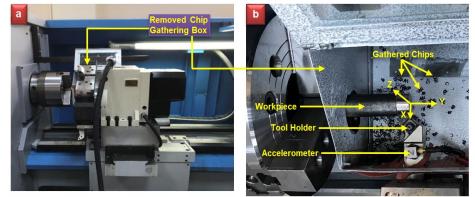


Figure 4. CNC Turning machine and experimental setup a) General view b) Gathering box

Table 1. Selected parameters and experiment plan

| Exp No | FeedRate mm/rev | Depth of Cut mm | CSR (G=a/f) | Rake Angle (α°) | Exp No | FeedRate mm/rev | Depth of Cut mm | CSR (G=a/f) | Rake Angle (α°) |
|---|---|---|---|---|---|---|---|---|---|
| 1 | 0.1 | 1 | 10 | 6 | 24 | 0.3 | 1.5 | 5 | 15 |
| 2 | 0.1 | 1 | 10 | 10 | 25 | 0.4 | 1.5 | 3.75 | 6 |
| 3 | 0.1 | 1 | 10 | 15 | 26 | 0.4 | 1.5 | 3.75 | 10 |
| 4 | 0.2 | 1 | 5 | 6 | 27 | 0.4 | 1.5 | 3.75 | 15 |
| 5 | 0.2 | 1 | 5 | 10 | 28 | 0.5 | 1.5 | 3 | 6 |
| 6 | 0.2 | 1 | 5 | 15 | 29 | 0.5 | 1.5 | 3 | 10 |
| 7 | 0.3 | 1 | 3.33 | 6 | 30 | 0.5 | 1.5 | 3 | 15 |
| 8 | 0.3 | 1 | 3.33 | 10 | 31 | 0.1 | 2 | 20 | 6 |
| 9 | 0.3 | 1 | 3.33 | 15 | 32 | 0.1 | 2 | 20 | 10 |
| 10 | 0.4 | 1 | 2.5 | 6 | 33 | 0.1 | 2 | 20 | 15 |
| 11 | 0.4 | 1 | 2.5 | 10 | 34 | 0.2 | 2 | 10 | 6 |
| 12 | 0.4 | 1 | 2.5 | 15 | 35 | 0.2 | 2 | 10 | 10 |
| 13 | 0.5 | 1 | 2 | 6 | 36 | 0.2 | 2 | 10 | 15 |
| 14 | 0.5 | 1 | 2 | 10 | 37 | 0.3 | 2 | 6.67 | 6 |
| 15 | 0.5 | 1 | 2 | 15 | 38 | 0.3 | 2 | 6.67 | 10 |
| 16 | 0.1 | 1.5 | 15 | 6 | 39 | 0.3 | 2 | 6.67 | 15 |
| 17 | 0.1 | 1.5 | 15 | 10 | 40 | 0.4 | 2 | 5 | 6 |
| 18 | 0.1 | 1.5 | 15 | 15 | 41 | 0.4 | 2 | 5 | 10 |
| 19 | 0.2 | 1.5 | 7.5 | 6 | 42 | 0.4 | 2 | 5 | 15 |
| 20 | 0.2 | 1.5 | 7.5 | 10 | 43 | 0.5 | 2 | 4 | 6 |
| 21 | 0.2 | 1.5 | 7.5 | 15 | 44 | 0.5 | 2 | 4 | 10 |
| 22 | 0.3 | 1.5 | 5 | 6 | 45 | 0.5 | 2 | 4 | 15 |
| 23 | 0.3 | 1.5 | 5 | 10 | | | | | |

The vibration values were recorded on the computer by using a data logger and fiber cable with the help of an NI-9230 C series accelerometer device. The measurement was carried out between -30g, and +30g. The sensor was fixed on the tool holder using a cohesive. Moreover, the tool holder, the chuck of the CNC lathe machine, the surface of the machined sample, and the insert tool are demonstrated in Figure 4. The vibration values were measured on X, Y, and Z coordinates matching with the

direction on the sensor of the accelerometer as seen in Figure 4. During the experimental procedure, every sample was machined 70mm in length in one pass, but in total, the specimens were machined 140mm in length in two passes as in conditions shown in Table 1.

Three different rake angles were selected as 6°, 10°, and 15° at 75 rpm constant cutting speed. Additionally, cutting tools, comprised of W, Ti, and Ta carbides and Co as a binder, were employed. However, feed rate (f) and depth of cutting (a) were selected according to the values of CSR (G=a/f). CSR, namely G, values were arranged as 5, 7.5, 10, 15, and 20, depending on the selected values of feed rates and cutting depths. According to the rake angle, three different kinds of inserts, WNMG 060408E, with 6°, 10°, and 15° rake angles were used in experiments, respectively, and one tool holder with serial number MNLNR 2525 M08. Inserts with 0.8mm of nose radius and tool holder are demonstrated in Figure 5a, Figure 5b, and Figure 5c.
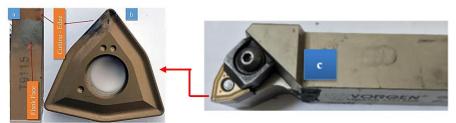


Figure 5. a) The flank face and cutting-edge of the insert, b) the head view and cutting-edge of the insert, c) tool holder for WNMG inserts

The AISI 1050 steel samples were prepared in Ø30mm in diameter and 150mm in length. Before the experimental procedure, each sample was pre-machined in a pass (aO) and the diameter of the sample was decreased to Ø29mm as seen in Figure 6. Then, in the experimental procedure, each sample was machined at selected parameters, especially in cutting depths as demonstrated in Table 1 with 70mm length for each pass, but two passes in total. The values of a1 and a2 passes were equal for each sample. The 1 and 2 indices only indicate the pass numbers. The volume of the removed chips on each sample was calculated by using the selected parameters as cutting depth and machining length. The calculated CCF was derived with the ratio of the measured chip volume to the calculated volume of the removed chips. Although CCF has been calculated as the removed chip thickness (tc) to the un-cut chip thickness (t1) in literature in the present study the ratio of the measured volume of the removed chip to the calculated un-cut chip was taken into account for calculating CCF values.
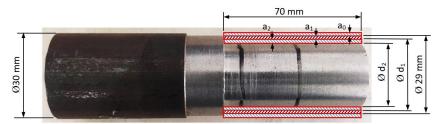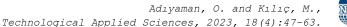


Figure 6. The size of samples employed in experimental procedure

### 3.5. Analysing and Measuring Methods

The chip morphology was investigated by metallographic studies. For this purpose, an FEI QUANTA 25° FEG scanning electron microscope (SEM) and macro photo camera were employed. The chip morphology was

demonstrated by a scanning electron microscope (SEM). SEM-EDX analysis was performed by utilizing a Philips XL-30S FEG. The machined surface roughness of the samples was measured at a sampling distance of 0.8mm utilizing a TIME TR 20° portable device.
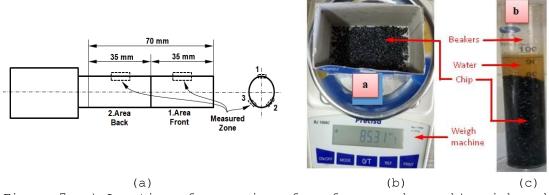


|  (a)  |  (b)  |  (c)  |

Figure 7. a) Location of measuring of surface roughness b) weigh and c) volume of the removed chips

Surface roughness was measured in six different locations on the machined surface of the samples as seen in Figure 7a. The length of the measured surface was divided into two equal areas, each of which was 35 mm in length. Consequently, the arithmetic mean of the recorded values was considered for each sample. The method of measuring the volume of the removed chips is demonstrated in Figure 7b with the help of beakers and water. In the measuring method, at first, the beaker was filled up at the level of an integer number, and then the chips were filled in the beaker. The water rose from the first level after the sample had been placed into the beaker. Then the difference between the first level and the last level was calculated and taken into account. Therefore, the variation value between the last and the first water level in the beaker was accepted as the volume of the removed chips. Additionally, the weight of the removed chips was measured by using a digital scale, having 0.01 g precision, as seen in Figure 7c.

## 4. FINDINGS AND DISCUSSIONS
### 4.1. Analysing Chip Compression Factor in Orthogonal Cutting Mechanism

In the orthogonal cutting mechanism, the effect of shear angle on CCF at selected rake angles was 6°, 10°, and 15° for the experimental procedure as demonstrated in Figure 8. The CCF values for chip angles 6, 10, and 15 were approximately 1.7 to 2.5. Additionally, CCF alteration graphs, in Figure 8e, consistent with the graphs are as seen in Figure 8a and Figure 8b. However, the alteration of CCF values in Figure 8a was recorded theoretically with the help of Matlab, approximately between 1.1 and 11 for selecting the rake angle between 0º and 20º, as well as the shear angle between 15O and 45O. Furthermore, the changes in CCF graphs as seen in Figure 8f, according to the selected rake angles, show a consistent with the graphs as demonstrated in Figure 8c and Figure 8d.
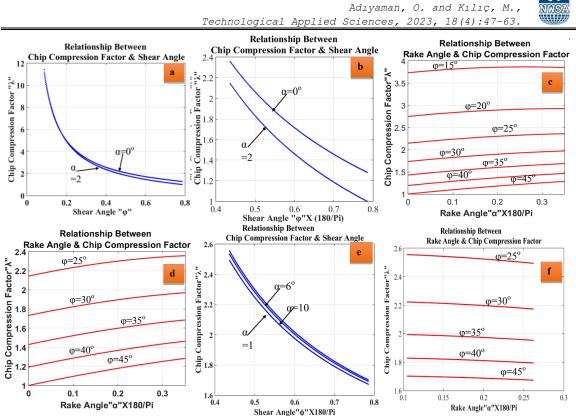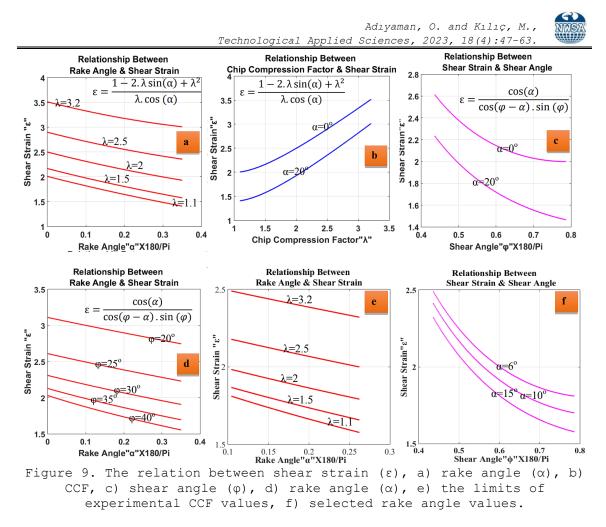
Figure 8. The relation between CCF, shear and rake angles a) φ=5°–45°,
b) φ=25°, c) α=0°–20° d) α=0°–20°, e) α=6°, 10°, 15°, f) φ=25°–45°

### 4.2. Analysing Chip Compression Factor and Shear Strain in Orthogonal Cutting Mechanism
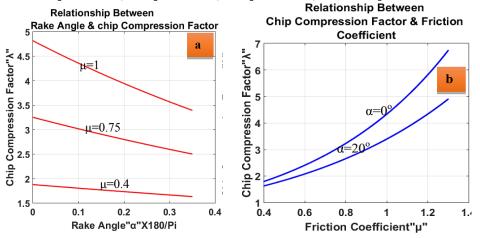
The correlation between rake angle (α), shear strain (ε), CCF (λ)-shear strain (ε), shear angle (φ), shear strain (ε), and rake angle (α) shear strain (ε) is demonstrated in Figure 9a, Figure 9b, Figure 9c, and Figure 9d, respectively. Figure 9 a shows the graphs of the relationship between rake angle (α) and shear strain (ε) depending on CCF. As the rake angle increases, shear strain regularly decreases but increases linearly with increasing CCF. As seen in Figure 9b, CCF value, and shear strain change regularly, but shear strain decreases linearly with increasing shear angle as shown in Figure 9c. Again the correlation between rake angle and shear strain can be seen in Figure 9d depending on shear angle. Furthermore, the relationship between rake angle and shear strain shows similarity as demonstrated in Figure 9a and d depending on CCF and shear angle, respectively. Furthermore, the alteration graphs of shear strain in the orthogonal cutting mechanism show a conformability depending on the shear angle as seen in Figure 9c and Figure 9f, also as demonstrated in Figure 9a, Figure 9d, and Figure 9e depending on rake angle. The shear strain graphs, which are obtained theoretically for the widely selected limit range for rake and shear angles, cover the graphical limits, which are derived for the selected rake angles in experimental studies

Figure 9. The relation between shear strain (ε), a) rake angle (α), b) CCF, c) shear angle (φ), d) rake angle (α), e) the limits of experimental CCF values, f) selected rake angle values.
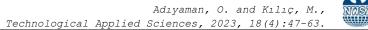
### 4.3. Analysing Chip Compression Factor (CCF) According to D'Alembert Motion Principle

When the CCF value is analyzed according to the friction coefficient with the help of Matlab, the graphs of the change, as seen in Figure 10 are achieved.

According to the graph in Figure 10a, CCF values regularly increase with increasing friction coefficient but decrease with increasing rake angle. As seen in Figure 10b, the influence of the friction coefficient on CCF is greater than the effect of the rake angle. According to the D'Alembert principle, CCF values are also compatible with theoretical values depending on the chip angles selected for the experimental study as seen in Figure 10a, Figure 10c, Figure 10b, and Figure 10d.
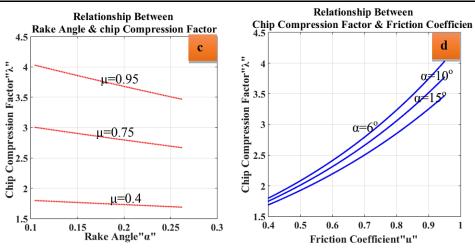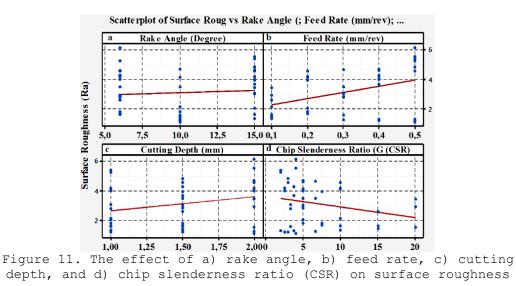
Figure 10. According to D'Alembert's principle the correlation between CCF and friction coefficient

## 4.4. Surface Roughness, Chip Compression Factor and Vibration

The surface roughness is one of the most significant results showing the quality of the machining and machinability in machining operations. With the scope of the study, the effects of rake angle, feed rate, cutting depth, and CSR on surface roughness were analyzed in turning AISI 1050 steel.



Figure 11. The effect of a) rake angle, b) feed rate, c) cutting depth, and d) chip slenderness ratio (CSR) on surface roughness
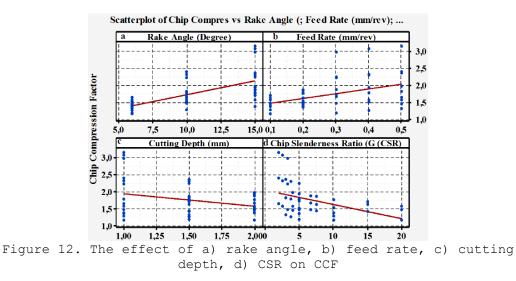
The influences of these parameters on the surface roughness are demonstrated in Figure 11 in the form of graphical curves. Surface roughness increased with increasing the rake angle regularly so less as that with the negligible amount as seen in Figure 11a. However, as the rake angle rises from 10° to 15°, surface quality deteriorates. Therefore, the maximum surface roughness value was recorded at a rake angle of 6° and the minimum at 10°. It is generally a proven rule that surface quality is deteriorated with increasing feed rate in machining operations. In the turning process of AISI 1050 steel material, the surface roughness was steadily increased by increasing the selected feed rate in the range of 0.1mm/rev to 0.5mm/rev as demonstrated in Figure 11b. However, this increment in surface roughness was severe while the feed rate progressed from 0.1mm/rev to 0.3mm/rev, but the increment severity was diminished when the feed rate altered from 0.3mm/rev to

0.5mm/rev. However, the surface roughness was degraded constantly with progressing cutting depth, as displayed in Figure 11c. This result shows that the depth of cut is not a function of surface roughness, in machining operations. The graph of the variance between cutting depth and surface roughness revealed a slope of approximately 45°. Therefore, the correlation difference between the depth of cut and surface roughness was better than other parameters.

The impression of CSR, which is known as the ratio of cutting depth to feed rate in the literature, is displayed in Figure 11d. As with the depth of cut, the surface roughness is degraded systematically by varying the CSR from 1 to 20. Since CSR is a parameter mainly dependent on the cutting depth, its influence on surface roughness was similar to that of the cutting depth. Especially with CSR values changing from 10 to 20, surface quality improved considerably. However, at CSR values, which are smaller than 5, surface roughness increased severely. According to the surface roughness criterion, it is recommended to select CSR values, namely the ratio of cutting depth to feed rate, greater than 10. The CCF indicates the evolution in the dimensions of the chips that are cut off by the cutting tool. Particularly, it is defined as the ratio of cut chip thickness to uncut chip thickness in the orthogonal cutting mechanism. It can also be represented as the ratio of the volume of the chip leaving the workpiece to the volume of the uncut chip. Therefore, CCF can also be considered as an indicator of the deformation impact that occurs in machining operations. The graphs of the evolution of CCF values with rake angle, feed rate, depth of cut, and CSR are displayed in Figure 12a, Figure 12b, Figure 12c, and Figure 12d, individually.



Figure 12. The effect of a) rake angle, b) feed rate, c) cutting depth, d) CSR on CCF
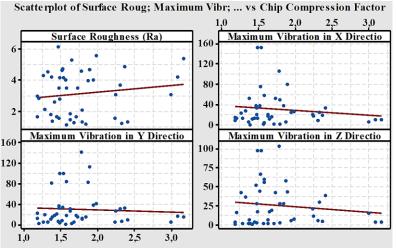
It is exhibited in Figure 12 a and b sequentially that CCF value progresses steadily with the development of both the rake angle and the feed rate. In the literature, it was found that the CCF value in the machining of steel materials was 1.8 [2]. In this experimental study, in which AISI 1050 steel was machined with the help of a lathe, CCF values were found to be between 1.2 and 3.2. According to CCF values, from the literature, CCF values, taken around 2, were found to be appropriate in this study. In Figure 12 a, it is observed that the graph of variation of CCF values shows diversity from approximately 1.5 to 2.5 with increasing rake angle to 15°. However, as the feed rate rises, the CCF difference graph rises steadily, while the feed rate is less than 0.2mm/rev CCF values are less than 2, but while the feed rate increments to 0.5mm/rev, CCF progress values received values greater than 2. As displayed in Figures 12c and d, sequentially, the plots of cutting depth

and the effect of CSR values on CCF are similar. Particularly, Figure 12c reveals that CCF values are dense in the range of 1.5 to 2 at 2mm cutting depth. In Figure 12d, it is observed that CCF values are in the range of approximately 1.5 to 2 for CSR values from 10 to 20. According to the 1.8 CCF value criterion in the literature, it was found that all cutting depths selected in the range of 1 to 2 were found to be appropriate, but CSR and rake angle values were higher than 10°, rake angles greater than 10° degrees and feed rates smaller than 0.2mm/rpm.

### 4.5. The Effect of CCF on Surface Roughness and Vibration

CCF is a parameter in the machining process. Depending on the difference in dimensions, after it is separated from the workpiece, especially the thickness of the chip is an important parameter. The influence of CCF on the surface roughness and maximum vibrations, which took place in directions of X, Y, and Z, are displayed in Figure 13a, Figure 13b, Figure 13c, and Figure 13d, individually. CCF value rose to 3.2, and the surface roughness progressed while the vibration value in X, Y, and Z directions decreased, regularly as seen in Figure 14. At large CCF values, the vibration values in the X, Y, and Z directions diminished, whereas in the CCF values smaller, in particular, in less than 1.7, the vibration values in all directions progressed significantly. According to surface roughness and vibration criterion, the most suitable CCF values were found to be between 1.7 and 2.3.



Figure 13. The effect of chip compression factor on surface roughness and vibration

### 4.6. The Alteration of CCF and Shear Strain

CCF, which is an indicator of deformation intensity in machining processes, is influenced by selected parameters such as feed rate, cutting depth, and chip angle.

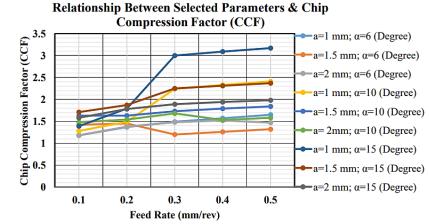**Relationship Between Selected Parameters & Chip Compression Factor (CCF)**

Figure 14. The effect of feed rate, cutting depth, and rake angle on
chip compression factor

Figure 14 reveals the graphical curves of the influence of feed
rate, cutting depth, and chip angle on CCF. According to the graphs of
the change in Figure 14, CCF progressed steadily as the feed rate rose.
Although the depth of the chip raised from 1mm to 2mm, CCF reduced
steadily, as the rake angle rose steadily from 6° to 15°, and it rose
linearly. The most appropriate parameters, according to the 1.8 CCF
criterion, were 15° rake angle and 2mm depth of cutting for all selected
feed rates. Additionally, 0.2mm/rev, 0.3mm/rev feed rates, 1mm, 1.5mm
depth of cutting, and 10°, and 15° rake angles were found to be the most
appropriate parameters. At the 6° rake angle, all CCF values were
recorded as less than 1.5 for all selected parameters. As seen in Figure
15, theoretically achieved CCF values, according to Equation 4, are
compared with the CCF values, obtained by measuring the volumes of the
removed chips, which were obtained from the experimental study.
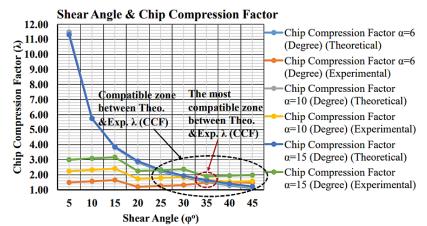
**Shear Angle & Chip Compression Factor**

Figure 15. The consistence of theoretical and experimental shear angle
depending on CCF

According to the theoretical and experimental CCF values, it is
detected that the actual shear angle is realized between 25° and 45° in
the turning process. However, the most consistent shear angle, between
analytical and experimental CCF values, was 35°. Therefore, in actual
machining operations, shearing of the chip occurs at a 35° inclination
angle.

According to Equation 7, the analytical and experimental variation
graphs of the amount of shear strain (ε) rake and shear angles are
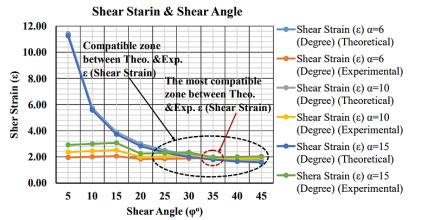displayed as in Figure 16 according to CCF values.

60

  
Figure 16. The consistence of theoretical and experimental shear angle depending on shear strain

While (t) analytical shear strain values are calculated theoretically according to rake and shear angles as displayed in Eq. (7), experimental CCF values, which were achieved according to Equation 4, are used in Equation 7 for experimental shear strain values. CCF variation graphs, as seen in Figure 15 in the shear strain (ε) charts, and in Figure 16, display a very similar variation. As displayed in the CCF graphs in Figure 15, the shear strain graphs in Figure 16 show that the actual shear angle in machining operations is between 25° and 45°. The consistent shear angle with the experimental results was 35 according to analytical and experimental values of both CCF and shear strain graphs.

## 5. CONCLUSION AND RECOMMENDATIONS

- Although CCF is a significant indicator of identifying the severity level of the deformation in machining operations, it has been studied scarcely in the literature. As the CCF value approached 1 and was bigger than about 2.3, the severity level of the deformation in the machining process, the amplitude of the vibration, and the cracks in the chip morphology, and the pitch size of the serration increased.
- The surface roughness was regularly reduced with rising rake angle, but the surface roughness progressed since it is known as a general rule that it increases with the feed rate.
- While the depth of cut and surface roughness change was directly proportional, CSR value and surface roughness difference were inversely proportional.
- CCF value rose, linearly with increasing of both rake angle and feed rate, but it regularly declined with the increase in both depths of cut and CSR values. Therefore, appropriate CSR values were to be higher than 10, especially 15 CSR value was recorded as the most appropriate.
- According to the criterion of surface roughness, for maximum vibration values transpiring in X, Y, and Z directions, the most suitable CCF values in turning of AISI 1050 steel were found to be around 2.
- According to the theoretical and experimental graphs of both CCF (λ) and shear strain (ε), it was determined that the turning process of AISI 1050 steel took place at approximately 35°. Furthermore, the shear strain (ε) and CCF (λ) evolved similarly.

- According to the chip morphology criterion, CCF values, which are compatible with the 1.8 CCF value obtained from the machining of steels from the literature studies, were found to be between 1.7 and 2.3.

**CONFLICT OF INTEREST**
The authors have no conflicts of interest to be disclosed.

**FINANCIAL DISCLOSURE**
The authors declare that this study has received no financial support.

**DECLARATION OF ETHICAL STANDARDS**
The authors of this article declare that the materials and methods used in this study do not require an ethical committee.

**REFERENCES**
[1]  Demir, Z. and Adiyaman, O., (2019). Investigation of influence of approach angle and chip slenderness ratio on vibration, chip formation and surface quality in turning of AISI 1050 steel. Journal of the Brazilian Society of Mechanical Sciences and Engineering, 41(10):467. Doi: 10.1007/s40430-019-1977-3.
[2]  Kronenberg, M., (1996). Machining science and application theory and practice for operation anddevelopment of machining processes. Arrowsmit Ltd. UK, 1-11.
[3]  Thamizhmanii, S. and Sulaiman, H., (2012). Machinability study using chip thickness ratio on difficult to cut metals by CBN cutting tool. Key Engineering Materials, 504:1317-1322. Doi:10.4028/www.scientific.net/KEÖ.504-506.1317.
[4]  Astakhov, V.P. and Shvets, S., (2004). The assessment of plastic deformation in metal cutting. Journal of Materials Processing Technology, 146:193-202.
[5]  Varga, G., (2012). Examination of shear angle in metal cutting. Production Processes and Systems, 1:71-78.
[6]  Silva, L.R., Abra, A.M., Faria. P., and Davim, J.P., (2012). Machinability study of steels in precisıon orthogonal cutting. Materials Research, 15(4):589-595. Doi:10.1590/S1516-14392012005000071.
[7]  Atlati, S., Haddag, B., Nouari, M., and Zenasni, M., (2011). Analysis of a new segmentation intensity ratio "SIR" to characterize the chip segmentation process in machining ductile metals. International Journal of Machine Tools & Manufacture, 51:687-700. Doi: 10.1016/j.ijmachtools.2011.05.007.
[8]  Ahearne, E. and Baron, S., (2017). Fundamental mechanisms in orthogonal cutting of medical grade cobalt chromium alloy (ASTM F75). CIRP Journal of Manufacturing Science and Technology, 19:1-6. Doi: 10.1016/j.cirpj.2017.02.001.
[9]  Ducobi, F., Lorphevre, E.R., and Filippi, E., (2016). Materials constitutive model and chip separation criterion influence on the modeling of Ti6Al4V machining with experimental validation in strictly orthogonal cutting condition. International Journal of Mechanical Sciences, 107:136-149. Doi: 10.1016/j.ijmecsci.2016.01.008.
[10]  Cui, X. and Guo, J., (2017). Effects of cutting parameters on tool temperatures in intermittent turning with the formation of serrated chip considered. Applied Thermal Engineering, 110:1220-1229. Doi: 10.1016/j.applthermaleng.2016.09.048.
[11]  Liu, H.Z., Wang, S.J., and Zong, W.J., (2019). Tool rake angle selection in micro-machining of 45 vol.%SiCp/2004Al based on its

brittle-plastic properties. Journal of Manufacturing Processes, 37:556-562. Doi: 10.1016/j.jmapro. 2018.12.030.

[12] Ye, G.G., Jiang, M.Q., Xue, S.F., Ma, W., and Dai, L.H., (2018). On the instability of chip flow in high- speed machining. Mechanics of Materials, 116:104-119. Doi: 10.1016/j.mechmat. 2017.02.006.

[13] Palacios, J.A., Olvera, D., Urbikain, G., Zuniga, A.E., Romero, O.M., Lacalle, L.N.L., Rodriguez, C., and Alfaro, H.M., (2018). Combination of simulated annealing and pseudo spectral methods for the optimum removal rate in turning operations of nickel-based alloys. Advances in Engineering Software, 115:391-397. Doi: 10.1016/j.advangsoft.2017.10.008.

[14] Duan, C., Dou, T., and Wang, M., (2009). Experimental Research of chip formation mechanism during high speed machining of hardened steel. International Journal of Advanced Engineering Applications (IJAEA), 2(3):17-21.

[15] Dahlman, P., Gunnberg, F., and Jacobson, M., (2004). The influence of rake angle, cutting feed and cutting depth on residual stresses in hard turning. Journal of Materials Technology, 147:181-184. Doi: 10.1016/j.matprotec.2013.12.014.

[16] Zhu, Z., Guo, K., Sun, J., Li, J., Liu, Y., Chen, L., and Zheng, Y., (2018). Evolution of 3D chip morphology and phase transformation in dry drilling Ti6Al4V alloys. Journal of Manufacturing Processes, 34:531-539. Doi: 10.1016/j.jmapro.2018.07.001.

[17] Outeiro, J.C., Costes, J.P., and Kornmeier, J.R., (2013). Cyclic variation of residual stress induced by tool vibration in machining operations. Procedia CIRP, 8:493-497. Doi: 10.1016/j.procir.2013.06.139.

[18] Adıyaman, O., (2021). Regression Modeling of the effect of chip slenderness ratio and cutting parameters on vibration. Gazi University Journal of Science Part C: Design and Technology, 9(4):661-678. Doi: 10.29109/gujsc.933055

[19] Liu, R., Eaton, E., Yu, M., and Kuang, J., (2017). An investigation of side flow during chip formation in orthogonal cutting. Procedia Manufacturing, 10:568-577. Doi: 10.1016/j.promfg.2017.07.053.

[20] Demir, Z. and Adıyaman, O. (2019). Investigation of the effect of Chip Slenderness Ratio and Cutting Tool Approach Angle on Vibration Amplitudes and Chip Morphology. Celal Bayar University Journal of Science, 15(4):423-431. Doi: 10.18466/cbayarfbe.629157.

[21] Martín Umbert, S., (2018). Cutting forces in turning operations. Bachelor's thesis, Universitat Politècnica de Catalunya.

[22] Cutting mechanics, http://www.me.unlv.edu/Undergraduate /coursenotes/wang/meg426/web/wk3/CLASS3.htm. Access Date: 17.12.2023.

[23] Mechanics of Cutting. chrome-extension:// efaidnbmnnnibpcajpcglclefindmkaj/https://home.iitk.ac.in/~vkjain /L6-TA-202%20MECHANICS%20OF%20CUTTING.pdf. Access Date: 17.12.2023.